Orbital-dependent self-energy effects and consequences for the superconducting gap structure in multiorbital correlated electron systems

Kristofer Björnson,[1,2] Andreas Kreisel,[3] Astrid T. Rømer,[1] and Brian M. Andersen[1]
[1]*Niels Bohr Institute, University of Copenhagen, Jagtvej 128, DK-2200 Copenhagen, Denmark*
[2]*Department of Physics and Astronomy, Uppsala University, Box 516, S-751 20 Uppsala, Sweden*
[3]*Institut für Theoretische Physik, Universität Leipzig, D-04103 Leipzig, Germany*

(Received 9 November 2020; accepted 28 December 2020; published 12 January 2021)

We perform a theoretical study of the effects of electronic correlations on the superconducting gap structure of multiband superconductors. In particular, by comparing standard RPA-based spin-fluctuation mediated gap structures to those obtained within the FLEX formalism for an iron-based superconductor, we obtain directly the feedback effects from electron-electron interactions on the momentum-space gap structure. We show how self-energy effects can lead to an orbital inversion of the orbital-resolved spin susceptibility, and thereby invert the hierarchy of the most important orbitals channels for superconducting pairing. This effect has important consequences for the detailed gap variations on the Fermi surface. We expect such self-energy feedback on the pairing gap to be generally relevant for superconductivity in strongly correlated multiorbital systems.

DOI: 10.1103/PhysRevB.103.024508

I. INTRODUCTION

The discovery of a growing class of unconventional multiband superconductors and the continuing development of high-resolution experimental probes of superconducting gap structures, highlight our need for theoretical models capable of quantitatively describing the detailed momentum structure of superconducting pairing. Thus, the modern theoretical objective is not only to locate the leading irreducible representation of the preferred gap function, but additionally to correctly describe all superconducting "gap details", consisting, for example, of the gap amplitude modulations and relative signs of the gaps on the participating Fermi surface sheets [1,2]. This ambitious goal has driven part of the research of iron-based superconductivity over the past decade, and remains currently very relevant, for example, for explaining superconductivity in multiband compounds such as infinite layer nickelates [3], FeSe [4], KFe_2As_2 [5], LiFeAs [6], UTe_2 [7], and Sr_2RuO_4 [8]. Since the superconducting gap structure is directly related to the mechanism of superconductivity, it serves as an important testing ground for different electron pairing scenarios. However, as exemplified in this paper, even within a given mechanism there are additional electron correlation effects that may severely affect the "gap details" of the resulting gap structure.

The importance of the strength of Coulomb repulsion in the formation of Cooper pairs relates to the overall question of whether electron-electron interactions are friend or foe of superconductivity. Within most unconventional pairing scenarios, repulsive interactions generate pairing in the first place [9–11], but there exists an optimal strength, since too strong interactions limit superconductivity. This issue has been discussed for cuprate superconductors where the single-band Hubbard Hamiltonian is the prime model under investigation [12]. However, for multiband systems, there exist additional complexity since the states at the Fermi level may exhibit different orbital character [13]. Thus, even though the Coulomb interaction is identical for electrons in the various active orbitals, the crystal structure and the corresponding band structure differentiates the orbitals at the Fermi level. At the bare level, one would expect the orbitals mainly contributing to Fermi level states to also dominate the pairing [14]. However, Coulomb repulsion may cause these same dominant orbital states to exhibit the largest self-energy, with potentially important implications for the resulting pairing state [14–23].

The issue of important self-energy feedback effects on the superconducting gap structure, has recently been intensely studied in relation to the material FeSe, featuring a Fermi surface consisting of small elliptical hole (electron) pockets near the Γ (M) point of the 2-Fe Brillouin zone [4,24,25]. In this compound, superconductivity materialises out of an electronic nematic phase and exhibits a remarkably large 90° rotational anisotropy [26]. The gap variation along the Fermi pockets is not straightforwardly explained by standard pairing models [14,26]. Specifically, the superconducting gap features very strong amplitude variations along the elliptical Fermi pockets and nearly vanishes around the vertex of the ellipses [26]. This gap structure is qualitatively different from that obtained from standard multiorbital random phase approximation (RPA) spin-fluctuation pairing, an approach that has been generally successful for many other iron-based materials [1,13,14,27]. Therefore it was hypothesized that additional correlation effects, e.g., orbital-dependent mass renormalizations, not included within the standard bare-RPA pairing formalism, might nontrivially affect the gap structure [14,19,28–30].

Here, by performing a direct comparison of the superconducting gap structures arising from bare-RPA versus the

self-consistent fluctuation exchange (FLEX) formalism [31], we can directly explore how electronic correlations can influence the resulting superconducting gap. Indeed, while both approaches subscribe to standard spin-fluctuation mediated superconductivity, the main difference between the methods is the inclusion of self-energy effects in the FLEX approach. While several earlier works have applied the self-consistent FLEX method to study pairing in iron-based superconductors [32–34], none have focused on the detailed orbital contributions and contrasted these to simpler methods neglecting self-energy effects in the pairing kernel. We find that while the overall symmetry class of the leading gap solution is not affected (for our case study), there are significant "gap details" that get strongly modified by self-energy effects. We trace the main difference between bare-RPA and self-consistent FLEX to the presence of a so-called orbital inversion, i.e., the fact that the orbital structure of the pairing kernel has been restructured by self-energy effects. This change of the orbital hierarchy in the contributions to the pairing naturally arise in multiorbital models where pairing and self-energy are caused by the same virtual processes, thereby rendering feedback effects important. We expect future computational schemes for pairing superior to FLEX to reach similar conclusions.

Finally, we discuss an approximate method of including the self-energy feedback effects in the pairing by incorporating orbital-dependent quasiparticle weights as proposed in Refs. [14,26]. We compare the results of this simpler approach to the full FLEX calculation.

II. MODEL AND METHOD

The model consists of a five-orbital tight-binding Hamiltonian H_0 including all relevant five Fe d orbitals $[d_{xy}, d_{x^2-y^2}, d_{xz}, d_{yz}, d_{3z^2-r^2}]$, and onsite interactions via the standard Hubbard-Hund term H_I

$$\begin{aligned} H &= H_0 + H_I \\ &= \sum_{ij\sigma}\sum_{qt} t_{ij}^{tq} c_{it\sigma}^\dagger c_{jq\sigma} \\ &\quad + U\sum_{it} n_{it\uparrow}n_{it\downarrow} + U'\sum_{i,t<q}\sum_{\sigma\sigma'} n_{it\sigma}n_{iq\sigma'} \\ &\quad + J\sum_{i,t<q}\sum_{\sigma\sigma'} c_{it\sigma}^\dagger c_{iq\sigma'}^\dagger c_{it\sigma'}c_{iq\sigma} \\ &\quad + J'\sum_{i,t\neq q} c_{it\uparrow}^\dagger c_{iq\downarrow}^\dagger c_{it\downarrow}c_{iq\uparrow}, \end{aligned} \tag{1}$$

with interaction parameters U, U', J, J' given in the notation of Kuroki *et al.* [27] fulfilling the relations $U' = U - 2J$ and $J = J'$. Here q and t are orbital indices and i, j denote Fe-atom sites. The kinetic part, H_0, is identical to that used in Ref. [35] consisting of a DFT-derived five-band model generated for LiFeAs. We choose a band relevant for LiFeAs since this material does not exhibit magnetic and nematic instabilities, but stress that the discussion below is general, and should be of relevance also to other multiband unconventional superconductors. The detailed band structure is not of crucial importance as long as it features multiple-orbital Fermi surface sheets.

The single-particle Green's function is given by

$$G(\mathbf{k}, \omega_m)^{-1} = G^0(\mathbf{k}, \omega_m)^{-1} - \Sigma(\mathbf{k}, \omega_m), \tag{2}$$

where the bare Green's function is $G^0(\mathbf{k}, \omega_m) = [i\omega_m - H_0(\mathbf{k}) + \mu]^{-1}$, and the self-energy in orbital basis is given by

$$\begin{aligned} &\Sigma_{ps}(\mathbf{k}, \omega_m) \\ &\quad = \frac{1}{\beta N_q}\sum_{\mathbf{q},\Omega_m}\sum_{qt} V_{pqst}(\mathbf{q}, \Omega_m) G_{qt}(\mathbf{k}-\mathbf{q}, \omega_m - \Omega_m). \end{aligned} \tag{3}$$

Here, $V_{pqst}(\mathbf{q}, \Omega_m)$ refers to the effective particle-hole interaction given by

$$\begin{aligned} V_{pqst}(\mathbf{q}, \Omega_m) = \Bigg[&\frac{3}{2}U^S\chi^S(\mathbf{q}, \Omega_m)U^S + \frac{1}{2}U^C\chi^C(\mathbf{q}, \Omega_m)U^C \\ &- \left(\frac{U^C + U^S}{2}\right)\chi^0(\mathbf{q}, \Omega_m)\left(\frac{U^C + U^S}{2}\right)\Bigg]_{pqst}, \end{aligned} \tag{4}$$

with the charge- and spin-fluctuation parts of the RPA susceptibility defined by

$$\begin{aligned} \chi^C(\mathbf{q}, \Omega_m) &= [1 + \chi(\mathbf{q}, \Omega_m)U^C]^{-1}\chi(\mathbf{q}, \Omega_m), \\ \chi^S(\mathbf{q}, \Omega_m) &= [1 - \chi(\mathbf{q}, \Omega_m)U^S]^{-1}\chi(\mathbf{q}, \Omega_m), \end{aligned} \tag{5}$$

with the matrices U^C and U^S given by

$$\begin{aligned} U^C_{pppp} &= U, \quad U^S_{pppp} = U, \\ U^C_{ppss} &= 2U' - J, \quad U^S_{ppss} = J, \\ U^C_{pssp} &= J', \quad U^S_{pssp} = J', \\ U^C_{psps} &= 2J - U', \quad U^S_{psps} = U'. \end{aligned} \tag{6}$$

The orbitally resolved susceptibility is given by

$$\begin{aligned} &\chi_{pqst}(\mathbf{q}, \Omega_m) \\ &\quad = -\frac{1}{\beta N_k}\sum_{\mathbf{k},\omega_m} G_{tq}(\mathbf{k}, \omega_m) G_{ps}(\mathbf{k}+\mathbf{q}, \omega_m + \Omega_m), \end{aligned} \tag{7}$$

where N_k is the number of $\mathbf{k}$ points and $\beta = 1/T$ denotes the inverse temperature. In Eq. (4), $\chi^0(\mathbf{q}, \Omega_m)$ refers to the standard bare multiorbital Lindhard function.

To obtain a self-consistent solution, we solve Eqs. (2)–(7) iteratively using the FLEX scheme shown in Fig. 1. The circle at the top corresponds to a bisection search that is used to find a chemical potential μ such that the particle number is kept at 6.0 within a numerical accuracy of 10^{-5}. To improve the numerical stability of the algorithm, the self-energy is also mixed with that obtained in the previous step using $\Sigma = (\Sigma_{\text{new}} + \Sigma_{\text{previous}})/2$, where Σ_{new} and Σ_{previous} are the self-energies obtained in the current and previous steps, respectively. The condition used to terminate the FLEX loop is that $\max(|G_{\text{new}} - G_{\text{previous}}|)/\max(|G_{\text{previous}}|) < 10^{-3}$, where G_{new} and G_{previous} are the Green's functions calculated in the current and previous steps, respectively. The calculations are done for $T = 100$ K, using a momentum space mesh with 30×30 points and truncating the Matsubara sums to include the 1000 smallest frequencies.

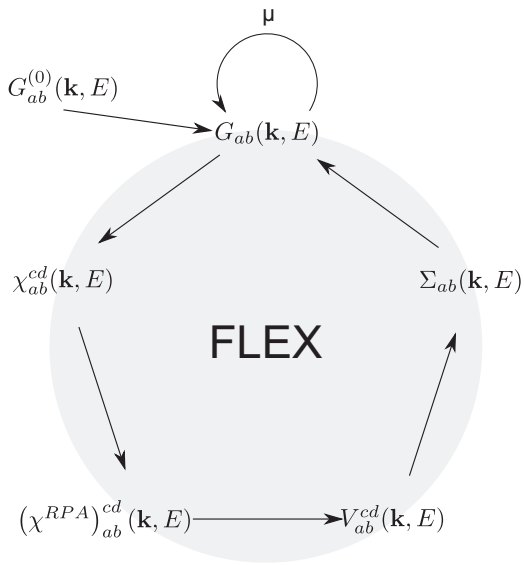

FIG. 1. Schematic illustration of the self-consistent FLEX scheme.

To compute the superconducting pair potential, we use the converged charge- and spin-susceptibilities to calculate [33]

$$V^{(SC)}_{pqst}(\mathbf{q}, \Omega_m) = \hat{U} + \tfrac{3}{2}U^S\chi^S(\mathbf{q}, \Omega_m)U^S - \tfrac{1}{2}U^C\chi^C(\mathbf{q}, \Omega_m)U^C, \quad (8)$$

where

$$\hat{U}_{pppp} = U, \quad \hat{U}_{ppss} = U', \quad \hat{U}_{pssp} = J, \quad \hat{U}_{psps} = J'. \quad (9)$$

We also obtained the spectral function through analytical continuation of the converged Green's function using the Padé approximation. More specifically, we use the continued fraction method [36,37].

The appearance of a superconducting instability at T_c can be found from solving the linearized gap equation,

$$-\frac{1}{V_G}\sum_{\mu}\int_{\mathrm{FS}_\mu} dS'\ \Gamma_{\nu\mu}(\mathbf{k}, \mathbf{k}')\frac{g_i(\mathbf{k}')}{|v_{\mathrm{F}\mu}(\mathbf{k}')|} = \lambda_i g_i(\mathbf{k}), \quad (10)$$

for the eigenvalues λ_i and the eigenvectors $g_i(\mathbf{k})$. Here, μ, ν are the band indices of the Fermi surface vectors $\mathbf{k}$, $\mathbf{k}'$, respectively, V_G is the area of a Brillouin zone and the magnitude of the Fermi velocity $|v_{\mathrm{F}\mu}(\mathbf{k})|$ weights the corresponding Fermi point. For this purpose, we project the pairing interaction at the lowest frequency into band space by

$$\Gamma_{\nu\mu}(\mathbf{k}, \mathbf{k}') = \mathrm{Re}\sum_{pqst} a^{p,*}_{\nu}(\mathbf{k})a^{t,*}_{\nu}(-\mathbf{k}) \times V^{(SC)}_{pqst}(\mathbf{k} - \mathbf{k}', \Omega_1)\, a^{q}_{\mu}(\mathbf{k}')a^{s}_{\mu}(-\mathbf{k}'), \quad (11)$$

where $a^{p}_{\mu}(\mathbf{k})$ are the matrix elements from the transformation from orbital space to band space. Here, we use as Hamiltonian $\tilde{H}(\mathbf{k}) = H_0(\mathbf{k}) + \frac{1}{2}[\Sigma(\mathbf{k}, \omega_0) + \Sigma(\mathbf{k}, \omega_0)^{\dagger}]$ where the Hermitian part of the self-energy matrix $\Sigma(\mathbf{k}, \omega_0)$ at the lowest Matsubara frequency ω_0, Eq. (3) is considered, a very good approximation at the Fermi level. The leading instability, identified by the largest eigenvalue λ_i is strictly speaking only correctly identified exactly at the critical temperature T_c, thus also the superconducting order parameter $\Delta(\mathbf{k})$ is proportional to $g_i(\mathbf{k})$ in this regime. We contrast this calculation to two usual spin-fluctuation calculations where the effective interaction is obtained within RPA without self-energy corrections [13], and an approach where the effect of correlations is included via quasiparticle weights in the susceptibility that enters RPA and the projection to band space given in Eq. (11) [14].

III. RESULTS

The role of electron correlations on the band structure of FeSCs has been studied theoretically by application of a variety of different methods [38–41]. In particular, both local and nonlocal self-energy effects on the Fermi surface have been explored and compared to experiments, and LiFeAs has played a prominent role in this exploration [35,42–51]. Figure 2 compares the bare electronic structure to the one described by the FLEX approach including the self-energy from Eq. (3) with $U = 1.2$ eV and $J = 0.15$ eV. In Fig. 2(c), we show the associated low-energy band structure along a standard high-symmetry momentum cut, again comparing the bare eigenenergies to the spectral density as extracted from the total spectral function continued to the real axis by use of the Padé approximation. Figure 2(a) displays the bare Fermi surface, whereas Fig. 2(b) shows the Fermi surface as obtained by utilizing the approximate Hamiltonian $\tilde{H}(\mathbf{k})$. In Fig. 2(c), the physical spectral density is compared to the band structure arising from both $H_0(\mathbf{k})$ and $\tilde{H}(\mathbf{k})$. As seen, the latter exhibits good overall agreement with high spectral intensity at low energies. From Fig. 2, it is evident that the main effect of $\Sigma_{ps}(\mathbf{k}, \omega_m)$ is to slightly modify the Fermi surface, causing smaller (larger) electron (hole) pockets. In addition, the second hole pocket around Γ acquires a "flower" shape. Such Fermi surface changes due to a momentum-dependent self-energy have been investigated in detail previously [22,32,34,49,52] and will not be further elaborated here. Instead, we focus on the modifications of the pairing structure from interactions.

Thus, we turn to a discussion of the superconducting gap structure, contrasting the bare RPA case to the FLEX situation including self-energy corrections. In the RPA calculation, the interaction parameters have to be considered as effective values, leading to a nominally smaller critical value for the Stoner instability. We therefore adjust the value of U such that the resulting eigenvalues λ in the pairing calculations are almost identical, leading to $U = 0.9$ eV for the RPA case. In Fig. 3, we display both the gap along the Fermi surface pockets [Figs. 3(a) and 3(c)] and the real-space orbital structure of the resulting gap function [Figs. 3(b) and 3(d)]. As seen, both gap structures support an $s\pm$ superconducting gap solution. However, there are significant effects of the self-energy on the "gap details." First of all, as seen from both the momentum-space plots and the real-space plots, the d_{xy} orbital contribution is significantly reduced in the FLEX case. This is evident from comparison of the relative strength of the intra-orbital pairing seen in the top left square of Figs. 3(b) and 3(d). In addition, this reduction is evident from the very weakened gap amplitude in d_{xy}-dominated segments of the

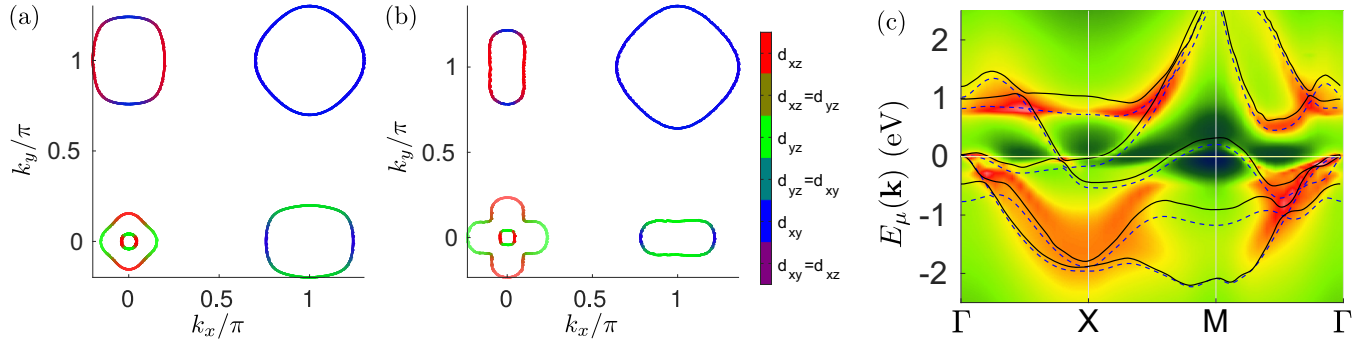

FIG. 2. (a) Fermi surface of the bare model. (b) Fermi surface of the correlated model with self-energy corrections and (c) Spectral function (color map) from the converged FLEX calculation for the same parameters as in (b), together with the unrenormalized bands (blue dashed) and the bands as obtained from adding the Hermitian part of the self energy (black).

Fermi surface, as seen from comparing Figs. 3(a) and 3(c). Essentially the blue sections of the Fermi surface shown in Fig. 2(b) have been "washed out."

In band space, the hierarchy of the gaps remains the same, e.g., the inner Γ-centered hole pocket exhibits the largest gap in both Figs. 2(a) and 2(c). The reduction of d_{xy}-dominated pairing renders the gap at the M point very small in the FLEX case, and it boosts the gap amplitude modulation on pockets exhibiting mixed orbital content, particularly those containing d_{xy}-dominated sections. This is seen most clearly from the electron pockets centered at the X and Y points in Fig. 3(c). We additionally show the gap structure projected to orbital space and Fourier transformed to real space, Figs. 3(b) and 3(d) for the two calculations. Each block represents the pairing in a certain orbital component $\Delta_{ps}(\mathbf{r})$, where the onsite pairing $\mathbf{r} = 0$ is represented by the center square of each block, and bond order parameters by the appropriate squares away from the center. Indeed, one can note that the $d_{xy} - d_{xy}$ block is strongly suppressed for the FLEX calculation [panel (d)] such that the $d_{xz} - d_{xz}$ and $d_{yz} - d_{yz}$ components dominate the FLEX result.

As a particular feature, we point out the structure of two blocks in the pairing field for the conventional calculation, Fig. 3(b). In the $d_{xz} - d_{xz}$ [$d_{yz} - d_{yz}$] block, the $\mathbf{r} = (\pm 1, 0)$ [$\mathbf{r} = (0, \pm 1)$] bond order $\Delta_{xz,xz}(\pm 1, 0)$ [$\Delta_{yz,yz}(0, \pm 1, 0)$] is small, but has opposite sign compared to the $\mathbf{r} = (0, \pm 1)$ [$\mathbf{r} = (\pm 1, 0)$] bond order $\Delta_{xz,xz}(0, \pm 1)$ [$\Delta_{yz,yz}(\pm 1, 0)$]. Formally, the nearest-neighbor pairing in the d_{xz} [d_{yz}] orbitals can be decomposed into an s-wave contribution, $\tilde{\Delta}_s$, and a d-wave contribution, $\tilde{\Delta}_d$, such that $\Delta_{xz,xz}(\pm 1, 0) = \tilde{\Delta}_s - \tilde{\Delta}_d \approx -0.001$ and $\Delta_{xz,xz}(0, \pm 1) = \tilde{\Delta}_s + \tilde{\Delta}_d \approx 1.2$ [$\Delta_{yz,yz}(\pm 1, 0) = \tilde{\Delta}_s + \tilde{\Delta}_d$ and $\Delta_{yz,yz}(0, \pm 1) = \tilde{\Delta}_s - \tilde{\Delta}_d$]. The sign change of the bond order then implies that $\tilde{\Delta}_d$ is slightly larger than $\tilde{\Delta}_s$. The order parameter $\tilde{\Delta}_d$ encodes an orbital singlet pairing with $d_{x^2-y^2}$-form factor as for example worked out in Refs. [19,53] for a different compound. In the longer range pairing channels like, e.g., $\Delta_{xz,xz}(0, \pm 2)$ and $\Delta_{yz,yz}(0, \pm 2)$ the change of sign is more visible, even though the overall size of the pairing strength at these sites is much smaller compared to the nearest neighbor pairing strength. The orbital singlet nature of the gaps is suppressed in the FLEX calculation, as seen from Fig. 3(d). Here, all pairing amplitudes in the $xz - xz$ and $yz - yz$ blocks are positive (blue). This means that the orbital character of the gap is preferentially "tripletlike" although a small singlet component remains, as seen from the change in gap magnitude between, e.g., $\Delta_{xz,xz}(0, \pm 1)$ and $\Delta_{xz,xz}(\pm 1, 0)$.

What is the underlying reason for the modified superconducting gap structures seen from the comparison between Figs. 3(a) and 3(c)? In order to answer this question we need to dissect the pairing kernel giving rise to the Cooper pair structure. As evident from Eqs. (8)–(11), the most important ingredient is the spin susceptibility. In Fig. 4(a), we display the real-part of the static total spin susceptibility for the bare, RPA, and FLEX cases. As seen, the overall momentum

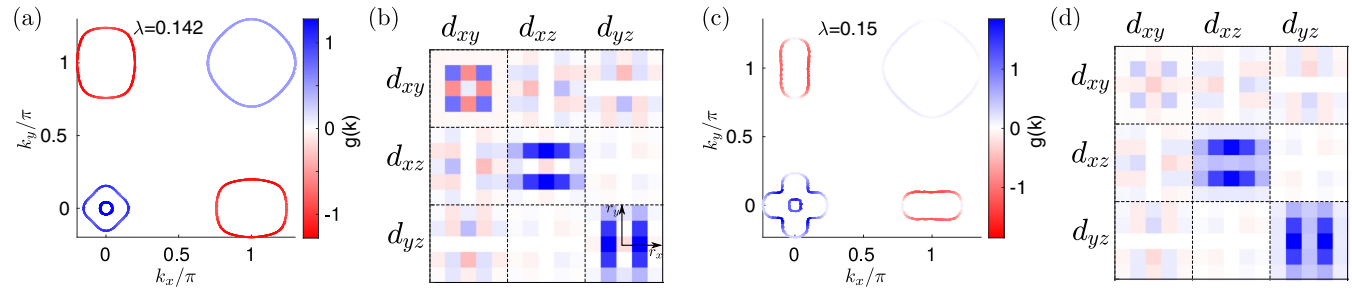

FIG. 3. (a) Superconducting gap symmetry function $g(\mathbf{k})$ for the pairing calculation in RPA ($U = 0.9$ eV and $J/U = 1/8$) together with (b) the transformation to real space pairing amplitudes and projection to orbital space. (c) the corresponding calculation using the pairing interaction as obtained from the self-consistent FLEX approach, $U = 1.2$ eV and $J/U = 1/8$. The latter yielding a much smaller pairing amplitude at the k points dominated by the d_{xy} orbital, which is also visible in the much smaller pairing amplitudes in the d_{xy}-d_{xy} channel (first square) of (d).

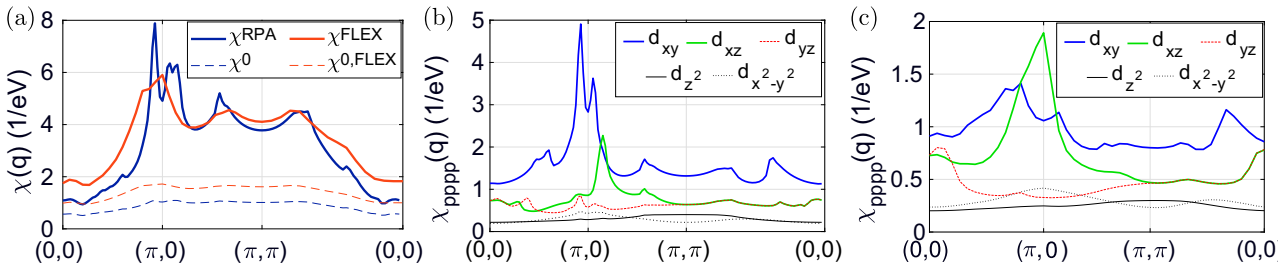

FIG. 4. (a) Comparison of the physical susceptibility as obtained from a non-self-consistent RPA calculation ($U = 0.86$ eV) and the self-consistent FLEX approach, $U = 1.2$ eV and $J = 0.15$ eV. (b) orbitally resolved susceptibility of the non-self-consistent approach showing the dominant d_{xy} contribution that gives rise to the peak at $(\pi, 0)$ and (c) corresponding orbitally resolved susceptibilities from the FLEX approach with dominant d_{yz} contribution at the same momentum transfer of $(\pi, 0)$.

structure is preserved, and FLEX merely tends to smear out the peak structure as a direct result of the self-energy. However, as seen from a comparison of the orbital-resolved susceptibilities in Figs. 4(b) and 4(c), an orbital inversion has taken place near $X = (\pi, 0)$ (and similarly near Y, not shown). In the FLEX case, the dominant susceptibility is found in the d_{xz}/d_{yz} channel, as opposed to the d_{xy} orbital channel for the bare-RPA case, thereby fundamentally restructuring the dominant pair scattering contributions to superconducting pairing. This orbital inversion of the susceptibility components is the main reason for the differences between the bare-RPA and FLEX superconducting gaps. The orbital inversion arises quite naturally in FLEX, since the same physical processes are involved in pairing and the self-energy. Thus, for systems close to magnetic instabilities where the spin susceptibility (bubble and ladder diagrams) is expected to be particularly important, incorporating the self-energy feedback effects of the susceptibility is crucial for obtaining a correct description of the "gap details." At present it remains to be seen whether future experiments, e.g., RIXS, may be able to selectively probe the orbital content of the spin susceptibility and compare this to calculations based on the bare band structure to verify the existence of such self-energy-generated orbital inversion.

As a function of increased interaction parameters U and J, both RPA and the FLEX approximation exhibit an instability of a magnetic state. In general, the self-energy in the FLEX approach tends to broaden the peaks of the susceptibility, thereby pushing the Stoner instability to a larger critical interaction strength. The orbital inversion, and the concomitant effects on the superconducting gap structure, discussed above are found in this enlarged large-U regime, and the results presented here are robust in this regime. At weak interaction strengths, the FLEX results resemble the bare-RPA results. Finally, we stress that for other bands the self-energy effects may not be as simple as an orbital inversion, especially if the momentum positions of the dominant peaks in the susceptibilities shift.

The result discussed above, exhibiting a strongly suppressed gap on the d_{xy}-dominated Fermi surface sections, is an example of what has been dubbed orbital-selective superconductivity. A "poor man's" version to incorporate the self-energy effects has been proposed, e.g., in Refs. [14,26,54,55] applied to FeSe and also in Ref. [8] applied to Sr_2RuO_4. In this method, quasiparticle weight renormalizations are simply included at the level of the single-particle Green's function. In this way, orbitals expected to be exposed to the largest self-energy effects, thereby experiencing the most suppressed quasiparticle weights, are naturally suppressed in their contributions to the superconducting pairing kernel.

We demonstrate this effect in the following; we can extract the approximate FLEX quasiparticle weights directly from the calculated self-energy by $Z_\alpha(\mathbf{k}) \approx [1 - \mathrm{Im}\,\Sigma_{\alpha\alpha}(\mathbf{k}, \omega_0)/\omega_0]^{-1}$, with $\omega_0 = \pi T$ [33,34]. This procedure yields $Z_{xy} \approx 0.52$ and $Z_{xz} = Z_{yz} \approx 0.6$ when evaluated at their relevant Fermi surface points, for the current FLEX case with $U = 1.2$ eV and $J = 0.15$ eV. Note that the relevant quasiparticle weights are only those for the d_{xy}, d_{xz}, d_{yz} orbitals. The two other orbitals have negligible weight on the Fermi surface and therefore their values do not influence the result for the pairing [14] and these orbitals contribute much less to the susceptibility, see Fig. 4(b). For the case of FeSCs, it is well-known from a wide range of methods that indeed Z_{xy} exhibits the largest reduction compared to the other four $3d$ orbitals [39–42,56,57]. In terms of the FLEX method, the fact that the d_{xy} orbital exhibits the largest mass renormalization for FeSCs was studied in detail, e.g., in Refs. [33–35].

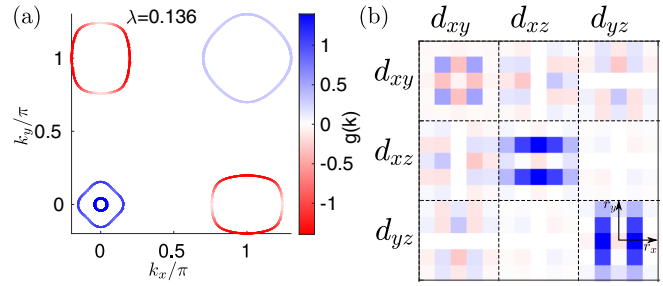

FIG. 5. (a) Superconducting gap symmetry function $g(\mathbf{k})$ for the pairing calculation using a modified spin-fluctuation pairing calculation with $U = 2.5$ eV and $J/U = 1/8$, and quasiparticle weights $Z_{xy} = 0.52$, $Z_{xz/yz} = 0.6$, $Z_{x^2-y^2} = 0.8$, and $Z_{z^2} = 0.72$ as deduced from the FLEX calculation. (b) Corresponding real-space pairing amplitudes showing small pairing contributions in the d_{xy} channel, while preserving the sign change in the next-nearest-neighbor pairing amplitudes of the d_{xz} and d_{yz} orbital components, i.e., $\Delta_{xz,xz}(0, \pm 2) - \Delta_{xz,xz}(\pm 2, 0) = -[\Delta_{yz,yz}(0, \pm 2) - \Delta_{yz,yz}(\pm 2, 0)]$.

Using the above-extracted values for the quasiparticle weights to renormalize the susceptibility and projection matrices of the usual RPA method leads to the superconducting gap structure shown in Fig. 5 where we have chosen the effective interaction ($U = 2.5$ eV) such that, again, the eigenvalue for the pairing calculation matches the one from the previous FLEX calculation; this choice, however, does not alter the result of the order parameter $g(\mathbf{k})$. As seen, including a reduced weight on the d_{xy} orbital qualitatively reproduces the FLEX very well (except for some details, e.g., the orbital-singlet pairing amplitude is not appropriately suppressed, $\tilde{\Delta}_d > \tilde{\Delta}_s$).

IV. DISCUSSION AND CONCLUSIONS

The work presented here is related to another recent theoretical study of momentum-dependent quasiparticle renormalization on the gap structure of FeSCs [22]. In Ref. [22], a one-loop FLEX calculation was presented, and it was explored how the inclusion of quasiparticle renormalizations $Z(\mathbf{k})$ alter the "gap details" along the relevant Fermi surface sheets. In agreement with the current work, the d_{xy} dominated part of the electron pockets were suppressed compared to the bare-RPA approach. However, no gap reduction was found in Ref. [22] on the large d_{xy}-dominated hole pocket centered at M, as opposed to the findings reported in this work. The main methodological difference with respect to the current work is the inclusion of the full self-consistency loop incorporated here. This allows for (1) proper self-energy feedback effects on the susceptibilities entering the pairing kernel and (2) exploration of the regime of larger interactions U and J inaccessible to one-shot calculations. These properties are crucial for the orbital inversion discovered here, and cause the strongly suppressed pairing on all d_{xy}-dominated sections of the Fermi surface.

More generally, we expect that other strongly correlated multiorbital metals should exhibit similar self-energy effects of their gap structure. However, there may well also be other cases where the self-energy can severely alter the gap for other reasons, e.g., by restructuring the orbital content of the Fermi surface, or by fundamentally altering the dominant momentum structure of the spin susceptibility. In the latter case, one can expect that self-energy effects change the symmetry class of the leading pairing instability [22].

In summary, we have explored the role of electronic correlations on the superconducting gap structure in multiorbital systems. Specifically, we contrasted the gap structure obtained from standard bare-RPA with that generated within the FLEX formalism, including self-energy feedback effects on the superconducting pairing kernel. The main finding is the existence of an orbital inversion, caused by the self-energy, of the hierarchy of susceptibility channels contributing to the pairing. This reduces the gap on the strongest correlated orbitals. For the current band structure, this leads to a very small gap on the largest hole pocket, and a significantly enhanced gap amplitude modulation on the electron pockets. This demonstrates the relevance of self-energy feedback effects on the gap structure of multiorbital correlated metals.

ACKNOWLEDGMENT

We thank T. A. Maier and P. J. Hirschfeld for useful conversations. K.B. and B.M.A. acknowledge support from the Independent Research Fund Denmark Grant No. 8021-00047B.

[1] P. J. Hirschfeld, Using gap symmetry and structure to reveal the pairing mechanism in Fe-based superconductors, C. R. Phys. **17**, 197 (2016).

[2] A. Chubukov, Pairing mechanism in Fe-based superconductors, Ann. Rev. Condens. Matter Phys. **3**, 57 (2012).

[3] D. Li, K. Lee, B. Y. Wang, M. Osada, S. Crossley, H. R. Lee, Y. Cui, Y. Hikita, and H. Y. Hwang, Superconductivity in an infinite-layer nickelate, Nature (London) **572**, 624 (2019).

[4] A. Kreisel, P. J. Hirschfeld, and B. M. Andersen, On the remarkable superconductivity of FeSe and its close cousins, Symmetry **12**, 1402 (2020).

[5] K. Okazaki, Y. Ota, Y. Kotani, W. Malaeb, Y. Ishida, T. Shimojima, T. Kiss, S. Watanabe, C.-T. Chen, K. Kihou, C. H. Lee, A. Iyo, H. Eisaki, T. Saito, H. Fukazawa, Y. Kohori, K. Hashimoto, T. Shibauchi, Y. Matsuda, H. Ikeda, H. Miyahara, R. Arita, A. Chainani, and S. Shin, Octet-line node structure of superconducting order parameter in KFe_2As_2, Science **337**, 1314 (2012).

[6] M. P. Allan, A. W. Rost, A. P. Mackenzie, Y. Xie, J. C. Davis, K. Kihou, C. H. Lee, A. Iyo, H. Eisaki, and T.-M. Chuang, Anisotropic energy gaps of iron-based superconductivity from intraband quasiparticle interference in LiFeAs, Science **336**, 563 (2012).

[7] L. Jiao, S. Howard, S. Ran, Z. Wang, J. O. Rodriguez, M. Sigrist, Z. Wang, N. P. Butch, and V. Madhavan, Chiral superconductivity in heavy-fermion metal UTe_2, Nature (London) **579**, 523 (2020).

[8] A. T. Rømer, D. D. Scherer, I. M. Eremin, P. J. Hirschfeld, and B. M. Andersen, Knight Shift and Leading Superconducting Instability from Spin Fluctuations in Sr_2RuO_4, Phys. Rev. Lett. **123**, 247001 (2019).

[9] W. Kohn and J. M. Luttinger, New Mechanism for Superconductivity, Phys. Rev. Lett. **15**, 524 (1965).

[10] D. J. Scalapino, A common thread: The pairing interaction for unconventional superconductors, Rev. Mod. Phys. **84**, 1383 (2012).

[11] A. T. Rømer, T. A. Maier, A. Kreisel, I. Eremin, P. J. Hirschfeld, and B. M. Andersen, Pairing in the two-dimensional Hubbard model from weak to strong coupling, Phys. Rev. Res. **2**, 013108 (2020).

[12] T. A. Maier, M. Jarrell, and D. J. Scalapino, Pairing interaction in the two-dimensional Hubbard model studied with a dynamic cluster quantum Monte Carlo approximation, Phys. Rev. B **74**, 094513 (2006).

[13] S. Graser, T. A. Maier, P. J. Hirschfeld, and D. J. Scalapino, Near-degeneracy of several pairing channels in multiorbital models for the Fe pnictides, New J. Phys. **11**, 025016 (2009).

[14] A. Kreisel, B. M. Andersen, P. O. Sprau, A. Kostin, J. C. Séamus Davis, and P. J. Hirschfeld, Orbital selective pairing and gap structures of iron-based superconductors, Phys. Rev. B **95**, 174504 (2017).

[15] N. Arakawa and M. Ogata, Orbital-selective superconductivity and the effect of lattice distortion in iron-based superconductors, J. Phys. Soc. Jpn. **80**, 074704 (2011).

[16] Z. P. Yin, K. Haule, and G. Kotliar, Spin dynamics and orbital-antiphase pairing symmetry in iron-based superconductors, Nat. Phys. **10**, 845 (2014).

[17] R. Yu, J.-X. Zhu, and Q. Si, Orbital-selective superconductivity, gap anisotropy, and spin resonance excitations in a multiorbital t-J_1-J_2 model for iron pnictides, Phys. Rev. B **89**, 024509 (2014).

[18] R. Nourafkan, G. Kotliar, and A. M. S. Tremblay, Correlation-Enhanced Odd-Parity Interorbital Singlet Pairing in the Iron-Pnictide Superconductor LiFeAs, Phys. Rev. Lett. **117**, 137001 (2016).

[19] H. Hu, R. Yu, E. M. Nica, J.-X. Zhu, and Q. Si, Orbital-selective superconductivity in the nematic phase of FeSe, Phys. Rev. B **98**, 220503(R) (2018).

[20] T.-H. Lee, A. Chubukov, H. Miao, and G. Kotliar, Pairing Mechanism in Hund's Metal Superconductors and the Universality of the Superconducting Gap to Critical Temperature Ratio, Phys. Rev. Lett. **121**, 187003 (2018).

[21] S. Acharya, F. Jamet, D. Pashov, and M. van Schilfgaarde, Interplay between band structure and Hund's correlation to increase T_c in FeSe, arXiv:1908.08136.

[22] S. Bhattacharyya, P. J. Hirschfeld, T. A. Maier, and D. J. Scalapino, Effects of momentum-dependent quasiparticle renormalization on the gap structure of iron-based superconductors, Phys. Rev. B **101**, 174509 (2020).

[23] L. Fanfarillo, A. Valli, and M. Capone, Synergy between Hund-Driven Correlations and Boson-Mediated Superconductivity, Phys. Rev. Lett. **125**, 177001 (2020).

[24] A. E. Böhmer and A. Kreisel, Nematicity, magnetism and superconductivity in FeSe, J. Phys.: Condens. Matter **30**, 023001 (2018).

[25] A. I. Coldea and M. D. Watson, The key ingredients of the electronic structure of FeSe, Annu. Rev. Condens. Matter Phys. **9**, 125 (2018).

[26] P. O. Sprau, A. Kostin, A. Kreisel, A. E. Böhmer, V. Taufour, P. C. Canfield, S. Mukherjee, P. J. Hirschfeld, B. M. Andersen, and J. C. S. Davis, Discovery of orbital-selective cooper pairing in FeSe, Science **357**, 75 (2017).

[27] K. Kuroki, S. Onari, R. Arita, H. Usui, Y. Tanaka, H. Kontani, and H. Aoki, Unconventional Pairing Originating from the Disconnected Fermi Surfaces of Superconducting $LaFeAsO_{1-x}F_x$, Phys. Rev. Lett. **101**, 087004 (2008).

[28] L. Benfatto, B. Valenzuela, and L. Fanfarillo, Nematic pairing from orbital selective spin fluctuations in FeSe, npj Quantum Mater. **3**, 56 (2018).

[29] L. C. Rhodes, J. Böker, M. A. Müller, M. Eschrig, and I. M. Eremin, Non-local d_{xy} nematicity and the missing electron pocket in FeSe, arXiv:2009.00507.

[30] J. Kang, R. M. Fernandes, and A. Chubukov, Superconductivity in FeSe: The Role of Nematic Order, Phys. Rev. Lett. **120**, 267001 (2018).

[31] N. E. Bickers, D. J. Scalapino, and S. R. White, Conserving Approximations for Strongly Correlated Electron Systems: Bethe-Salpeter Equation and Dynamics for the Two-Dimensional Hubbard Model, Phys. Rev. Lett. **62**, 961 (1989).

[32] R. Arita and H. Ikeda, Is Fermi-surface nesting the origin of superconductivity in iron pnictides?: A fluctuation-exchange-approximation study, J. Phys. Soc. Jpn. **78**, 113707 (2009).

[33] H. Ikeda, R. Arita, and J. Kuneš, Phase diagram and gap anisotropy in iron-pnictide superconductors, Phys. Rev. B **81**, 054502 (2010).

[34] H. Ikeda, R. Arita, and J. Kuneš, Doping dependence of spin fluctuations and electron correlations in iron pnictides, Phys. Rev. B **82**, 024508 (2010).

[35] S. Bhattacharyya, K. Björnson, K. Zantout, D. Steffensen, L. Fanfarillo, A. Kreisel, R. Valentí, B. M. Andersen, and P. J. Hirschfeld, Nonlocal correlations in iron pnictides and chalcogenides, Phys. Rev. B **102**, 035109 (2020).

[36] H. J. Vidberg and J. W. Serene, Solving the Eliashberg equations by means of N-point Padé approximants, J. Low Temp. Phys. **29**, 179 (1977).

[37] K. S. D. Beach, R. J. Gooding, and F. Marsiglio, Reliable Padé analytical continuation method based on a high-accuracy symbolic computation algorithm, Phys. Rev. B **61**, 5147 (2000).

[38] T. Miyake, K. Nakamura, R. Arita, and M. Imada, Comparison of ab initio low-energy models for LaFePO, LaFeAsO, $BaFe_2As_2$, LiFeAs, FeSe, and FeTe: Electron correlation and covalency, J. Phys. Soc. Jpn. **79**, 044705 (2010).

[39] L. de' Medici, in *The Physics of Correlated Insulators, Metals, and Superconductors Modeling and Simulation*, edited by E. Pavarini, E. Koch, R. Scalettar, and R. M. Martin (Verlag des Forschungszentrum Jülich, Jülich, 2017), Vol. 7, pp. 377–398.

[40] A. van Roekeghem, P. Richard, H. Ding, and S. Biermann, Spectral properties of transition metal pnictides and chalcogenides: Angle-resolved photoemission spectroscopy and dynamical mean-field theory, C. R. Phys. **17**, 140 (2016).

[41] E. Bascones, B. Valenzuela, and M. J. Calderón, Magnetic interactions in iron superconductors: A review, C. R. Phys. **17**, 36 (2016).

[42] Z. P. Yin, K. Haule, and G. Kotliar, Magnetism and charge dynamics in iron pnictides, Nat. Phys. **7**, 294 (2011).

[43] C. Platt, R. Thomale, and W. Hanke, Superconducting state of the iron pnictide LiFeAs: A combined density-functional and functional-renormalization-group study, Phys. Rev. B **84**, 235121 (2011).

[44] J. Ferber, K. Foyevtsova, R. Valentí, and H. O. Jeschke, LDA + DMFT study of the effects of correlation in LiFeAs, Phys. Rev. B **85**, 094505 (2012).

[45] Y. Wang, A. Kreisel, V. B. Zabolotnyy, S. V. Borisenko, B. Büchner, T. A. Maier, P. J. Hirschfeld, and D. J. Scalapino, Superconducting gap in LiFeAs from three-dimensional spin-fluctuation pairing calculations, Phys. Rev. B **88**, 174516 (2013).

[46] T. Saito, Y. Yamakawa, S. Onari, and H. Kontani, Revisiting orbital-fluctuation-mediated superconductivity in LiFeAs: Nontrivial spin-orbit interaction effects on the band structure and superconducting gap function, Phys. Rev. B **92**, 134522 (2015).

[47] T. Saito, S. Onari, Y. Yamakawa, H. Kontani, S. V. Borisenko, and V. B. Zabolotnyy, Reproduction of experimental gap

structure in LiFeAs based on orbital-spin fluctuation theory: s_{++}-wave, $s_{\pm}$-wave, and hole-$s_{\pm}$-wave states, Phys. Rev. B **90**, 035104 (2014).

[48] F. Ahn, I. Eremin, J. Knolle, V. B. Zabolotnyy, S. V. Borisenko, B. Büchner, and A. V. Chubukov, Superconductivity from repulsion in LiFeAs: Novel *s*-wave symmetry and potential time-reversal symmetry breaking, Phys. Rev. B **89**, 144513 (2014).

[49] K. Zantout, S. Backes, and R. Valentí, Effect of Nonlocal Correlations on the Electronic Structure of LiFeAs, Phys. Rev. Lett. **123**, 256401 (2019).

[50] M. Kim, H. Miao, S. Choi, M. Zingl, A. Georges, and G. Kotliar, On the spatial locality of electronic correlations in LiFeAs, arXiv:2009.10577.

[51] D. D. Scherer, A. C. Jacko, C. Friedrich, E. Şaşıoğlu, S. Blügel, R. Valentí, and B. M. Andersen, Interplay of nematic and magnetic orders in FeSe under pressure, Phys. Rev. B **95**, 094504 (2017).

[52] L. Ortenzi, E. Cappelluti, L. Benfatto, and L. Pietronero, Fermi-Surface Shrinking and Interband Coupling in Iron-Based Pnictides, Phys. Rev. Lett. **103**, 046404 (2009).

[53] E. M. Nica and Q. Si, Multiorbital singlet pairing and $d+d$ superconductivity, npj Quantum Mater. **6**, 3 (2021).

[54] R. Zhou, D. D. Scherer, H. Mayaffre, P. Toulemonde, M. Ma, Y. Li, B. M. Andersen, and M.-H. Julien, Singular magnetic anisotropy in the nematic phase of FeSe, npj Quantum Mater. **5**, 93 (2020).

[55] A. Kreisel, B. M. Andersen, and P. J. Hirschfeld, Itinerant approach to magnetic neutron scattering of FeSe: Effect of orbital selectivity, Phys. Rev. B **98**, 214518 (2018).

[56] R. Yu and Q. Si, $U(1)$ slave-spin theory and its application to Mott transition in a multiorbital model for iron pnictides, Phys. Rev. B **86**, 085104 (2012).

[57] L. Fanfarillo, G. Giovannetti, M. Capone, and E. Bascones, Nematicity at the Hund's metal crossover in iron superconductors, Phys. Rev. B **95**, 144511 (2017).